Viscous Shock-Layer Solutions with Nonequilibrium Chemistry for Hypersonic Flows Past Slender Bodies

E. V. Zoby*
NASA Langley Research Center, Hampton, Virginia
K. P. Lee†
Old Dominion University, Norfolk, Virginia
R. N. Gupta‡
Scientific Research and Technology, Inc., Hampton, Virginia
and
R. A. Thompson§ and A. L. Simmonds¶
NASA Langley Research Center, Hampton, Virginia

A parametric study of laminar nonequilibrium heat transfer to slender vehicles is presented. The study includes the variation of velocity-altitude conditions, blunted cone half angles, and nose bluntness. The study includes cone angles of 6, 10, and 20 deg with corresponding nose radii of 0.125, 0.5, and 0.75 ft. The effect of vehicle attitude is also considered. The heating-rate results are presented as a ratio of the noncatalytic to the corresponding fully catalytic value to illustrate the maximum potential for a heating reduction in dissociated nonequilibrium flow at flight conditions. The largest cone angle produces the most nonequilibrium effects (lowest ratio value) at distances beyond 100 nose radii. An unexpected reversal of this trend is obtained in the fore-cone region. Calculations with the smaller cone angles yield the largest heating reduction in this region. For the smaller cone angles, these effects are attributed to a more rapid expansion of the flow resulting in freezing of the flow chemistry and larger percentages of dissociated species. Conditions of increased nose blunting are also shown to produce large reductions in the heating ratio for the smaller cone angles at relatively large downstream surface lengths. The present calculations also highlight the face that, unlike equilibrium flow, the nose radius and freestream density are not independent scaling parameters in nonequilibrium flow. The effects of nose radius, altitude (density), and wall temperature on the stagnation-point nonequilibrium heating are demonstrated. The distributions of the heat-reduction ratio are compared for a cone at angle of attack and an equivalent cone angle.

Nomenclature

C_i = mass fraction of ith species
L = vehicle length
Le = Lewis number
M = Mach number
Pr = Prandtl number
p = pressure
$\dot{q}$ = heating rate
$\bar{q}$ = heating ratios (Fig. 11)
R_n = nose radius
s = vehicle wetted length
T = temperature
u = velocity
x = vehicle axial length
α = angle of attack
ε = Reynolds number parameter (Ref. 14)
μ = viscosity
η = transformed coordinate normal to vehicle surface
ρ = density
θ_c = vehicle half angle

Subscripts

FC = fully catalytic
NC = noncatalytic
i = ith species
ref = reference condition
st = stagnation condition
w = wall
∞ = freestream

Presented as Paper 88-2709 at the AIAA Thermophysics, Plasmadynamics and Lasers Conference, San Antonio, TX, June 27-29, 1988; received Nov. 10, 1988; revision received Feb. 6, 1989.

*Aero-Space Technologist, Aerothermodynamics Branch, Space Systems Division. Associate Fellow AIAA.
†Graduate Student; currently at Scientific Research and Technology, Inc., Hampton, VA. Member AIAA.
‡Senior Scientist. Associate Fellow AIAA.
§Aero-Space Technologist, Aerothermodynamics Branch, Space Systems Division. Member AIAA.
¶Mathematician, Aerothermodynamics Branch, Space Systems Division. Member AIAA.

Introduction

THERE has been an increase in interest to improve both the understanding of viscous flowfield phenomena and also the computational capability for application to hypersonic slender bodies. This interest has been motivated by proposed transatmospheric vehicles[1,2] (TAV) whose trajectories will encompass a large range of freestream conditions. The low-altitude, high Reynolds number trajectory conditions require methods capable of predicting reliable laminar and turbulent heating rates in flowfields dominated by perfect gas or equilibrium-air chemistry. Recent studies[3,4] have presented results of computational fluid dynamic (CFD) techniques in good agreement with experimental flight and ground-test data and with results of other CFD methods. This phase of the TAV trajectory should provide the conditions that determine the primary thermal protection system for the vehicle. The high-altitude, low Reynolds number phase of the trajectories

requires computational procedures that include nonequilibrium gas chemistry as well as shock and wall slip and surface catalytic effects. An investigation[5] that extended the analysis of Ref. 4 to include slip effects has shown good comparison with available ground-test pressure, drag, and heat-transfer data. The low-density flow conditions are important to understand since the proposed missions may plan maneuvers at these conditions, and vehicle aerodynamics could be influenced significantly. In addition, a complete hypersonic flowfield analysis should include finite-rate chemistry capability since frozen or equilibrium flow represents only the very high- or low-altitude conditions, respectively.

Although the importance of nonequilibrium flow has been known for some time, the benefits to flight applications were first illustrated by the initial flights of the Space Shuttle. Wall temperature measurements and resulting heat-transfer rates to the Shuttle Orbiter have been demonstrated[6-10] to be lower than predicted equilibrium values. The flight data from the Catalytic Surface Experiment,[7] which was a Space Shuttle Orbiter experiment conducted by NASA Ames Research Center, have verified that the lower rates can be attributed primarily to the relatively noncatalytic nature of the thermal protection system and not to unknowns in freestream or flowfield quantities, and that some degree of chemical nonequilibrium persists to altitudes as low as 50 km. Finally, if the descent trajectory of a TAV is similar to that of the Shuttle (high angle-of-attack condition assists in reducing the entry velocities at high altitudes), a nonequilibrium calculation may be required to ascertain if only surface reradiation is sufficient or if an active cooling method is necessary to maintain desired material temperatures.

The altitude-velocity range as well as vehicle attitude and bluntness ranges for which nonequilibrium chemistry impacts laminar heat transfer to long slender vehicles are not well established. Recent studies[11,12] have presented limited results for these flow conditions. This paper presents a more extensive investigation of the influence of nonequilibrium flow effects to slender vehicles for ranges of nose radii and body half angles. Also, the impact of altitude-velocity variation, vehicle attitude, and surface temperature effects are considered.

Analysis

Basic Approach

For a complete, detailed analysis, a Navier-Stokes (NS) method may be desirable, but the NS solution procedures require prohibitive computer run times and storage requirements for a parametric study over long bodies. The viscous shock-layer (VSL) equations are a subset of the NS equations and are obtained by retaining terms up to second order in the inverse square root of the Reynolds number. The VSL equations were developed by Davis[13] and yield a simplified set of governing equations that are uniformly valid through the shock layer to moderately low Reynolds numbers.[5] The VSL method has been shown to provide results in good agreement with experimental data, e.g., Refs. 3, 4, and 14. As a result, the VSL method has been used extensively to study the effect of various physical phenomena (such as coupled radiation and ablation, turbulence, and nonequilibrium chemistry) on flowfield computations. Therefore, a recently developed VSL code is used for this study. Computed results based on this code have been shown[4] to yield good agreement with results of other CFD codes and flight and ground-test data for high Reynolds number flow conditions. The code was modified[5] for shock- and surface-slip conditions, and computed results were shown to be in good agreement with applicable ground-test data. A finite-rate chemistry option has been included in the present method. Since the flow governing equations are presented in detail in Refs. 12 and 14, these equations are not presented herein. A brief discussion of the boundary conditions, chemical kinetics, thermodynamics, and transport properties is presented.

Boundary Conditions

The boundary conditions at the shock are calculated by using the Rankine-Hugoniot relations and assuming the flow to be frozen at the freestream composition. The surface conditions are given by the classical wall boundary values and include for the nonequilibrium flow calculations of this paper:

Noncatalytic wall

$$\frac{\partial C_i}{\partial \eta} = 0 \tag{1}$$

Fully catalytic wall

$$C_{i,w} = C_{i,\infty} \tag{2}$$

The coupled effects of slip and surface catalycity are not included in this study. The results of Ref. 5 indicate that for ε, a Reynolds number parameter less than approximately 0.15, the effect of slip on the surface heat transfer is insignificant. The values of ε are less than this number for the present conditions.

Chemical Kinetics

For this study, a five-species (O_2, N_2, O, N, NO) air model is used. The chemical reaction model and the reaction-rate constants are based on the results presented by Blottner.[15] Ionization has not been included in the present study, since the effect should be negligible on the surface quantities for the present range of freestream conditions. A seven-species and an eleven-species model were used in a stagnation-region Navier-Stokes code for a recent flowfield study[16] of highly energetic flows characteristic of aeroassist orbital transfer vehicles (AOTV) entering the Earth's atmosphere.

Thermodynamic and Transport Properties

The thermodynamic properties of the specific heat and enthalpy for the five-species model are needed. These individual species properties are obtained from polynomial curve fits in terms of temperature. For temperatures to 6000 K, the data of Ref. 17 are used. From 5500–15,000 K, the source of the thermodynamic properties is Ref. 18. The data of Browne[19,20] provide the required information for temperatures from 14,500–30,000 K. An overlap of temperature from the data sources is used to establish smooth transitions of the data sets and to ensure continuous derivatives.

The transport properties of the individual species are also calculated by polynomial curve fits in terms of temperature for the data given by Yos.[21] Since the conditions of the present study do not encompass significant ionization levels, the semiempirical method of Wilke[22] is used to calculate the gas mixture viscosity. The gas mixture thermal conductivity is computed by the Mason and Saxena[23] relation. For the current study, a constant Lewis number of 1.4 is used, and a variable Prandtl number is computed.

Method of Solution

The method of solution for this VSL analysis is presented in detail in Refs. 4 and 12. An input shock is required as an initial guess for a VSL method, and the present technique uses either a perfect-gas VSL solution at a corresponding cone angle or the nonequilibrium solution for a slightly larger cone angle. The normal and global continuity equations are solved simultaneously for the pressure and normal velocity. This procedure was introduced in the investigation of Ref. 24. The density term is eliminated with an equation of state. The tangential momentum, energy (in terms of temperature), and the species continuity equations are solved in a successive manner. For the present method, the shock shape extending to a location beyond the shock-inflection point is globally iterated. Four global iterations of the flowfield region encompassing the shock inflection were performed for several condi-

tions, as noted in Ref. 12. The discrepancies in the values of the shock standoff distance and the slope based on results from the third and fourth global passes were found to be insignificant (less that 1%). Therefore, three global passes were generally used to obtain converged solutions for the purposes of this study. Downstream of this location, the initial shock shape is obtained by linear extrapolation of the previous values and is converged by local iterations. The present computational procedure for very long bodies is more time-efficient than the approach that globally converges the shock over the entire body. However, again for a few conditions of this investigation, the computed shock shape over the entire body was then globally iterated. No subsequent changes in the shock parameters or surface-measurable quantities were noted as might be expected. For this method, the shock derivative in the streamwise direction, rather than the shock standoff distance, as in Ref. 3, is smoothed after a global iteration.

Results and Discussion

In this section, a discussion based on comparisons of the present VSL code results and experimental heating data obtained during the first flights of the Space Shuttle is presented. A brief discussion of a comparison of slender-body calculations based on the present cody and a 3-D VSL nonequilibrium code is also presented. Murray and Lewis[25] extended the original VSL method to three dimensions and applied the code (VSL3D) to spherically blunted conical configurations. The VSL3D code was later modified to include nonaxisymmetric bodies[26] as well as to treat nonequilibrium chemistry[27] in the shock layer. This version (Ref. 27) of VSL3D is used in the present investigation to assess nonequilibrium flow effects at angle of attack. These comparisons should demonstrate the applicability of the code. The calculated results from the present parametric study are then presented. The results are provided primarily as a ratio of the noncatalytic heating rate to the corresponding fully catalytic value. This ratio demonstrates the maximum potential for a surface heating-rate reduction in the presence of dissociated nonequilibrium flow over a finite-catalytic surface.

Obviously, the actual heating-rate reduction is a function of the catalytic nature of the surface material or coating. The heating rate for a finite-catalytic wall would be greater than the one computed for a noncatalytic wall, and thus the actual heat reduction would be less than the values presented herein. The benefits derived from a surface with finite catalycity would increase as the present ratio decreases. As the flow chemistry tends toward a frozen or equilibrium state, the ratio of noncatalytic to fully catalytic surface heating approaches 1, and benefits of a finite-catalytic surface would not be realized. The computed results are presented for a range of cone half angles and nose radii. In addition, the effects of Mach number, altitude, and angle of attack on the nonequilibrium results are also considered in the analysis.

Comparisons with Previous Results

The Shuttle heat-transfer data obtained over an altitude range of 250,000–160,000 ft have been compared with results of detailed nonequilibrium codes.[6,9,10] Discrepancies of less that 15% were reported in Ref. 9. The axisymmetric VSL method[6] employed a hyperboloid with a computed half angle and nose radius to model the Shuttle windward-ray coordinates at a given angle of attack. The equivalent-hyperboloid concept has been used extensively in 2-D flow analyses to model the Shuttle windward-symmetry plane and has been shown[28–30] to yield good agreement with Shuttle flight- and ground-test data and equilibrium air heat-transfer predictions. Recent 3-D VSL Shuttle analyses[9,31] presented good agreement with the equilibrium and nonequilibrium 2-D analyses. Likewise, the nonequilibrium results of the present axisymmetric code using the equivalent hyperboloid concept have been

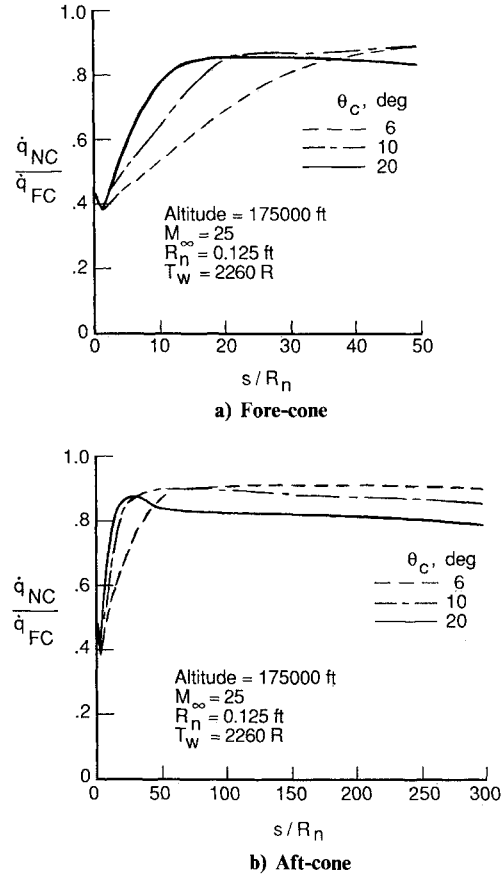

Fig. 1 Cone-angle effect on noneequilibrium heat-transfer distributions, $R_n = 0.125$ ft.

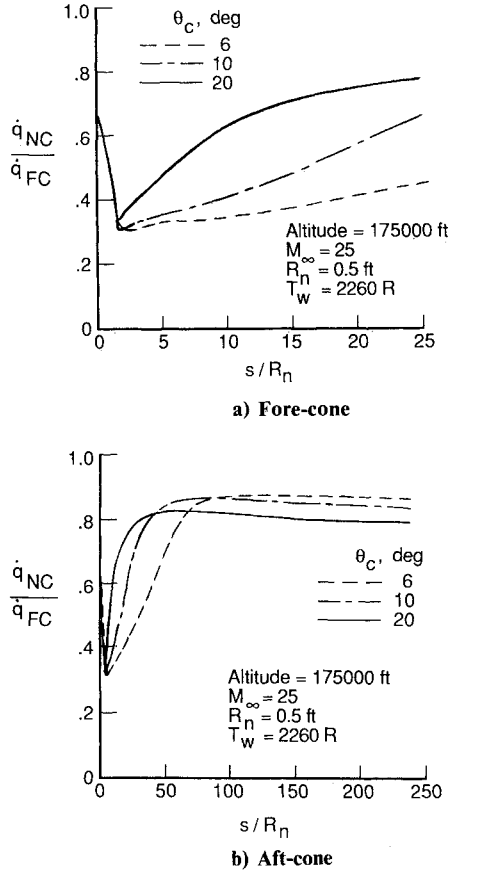

Fig. 2 Cone-angle effect on nonequilibrium heat-transfer distributions, $R_n = 0.5$ ft.

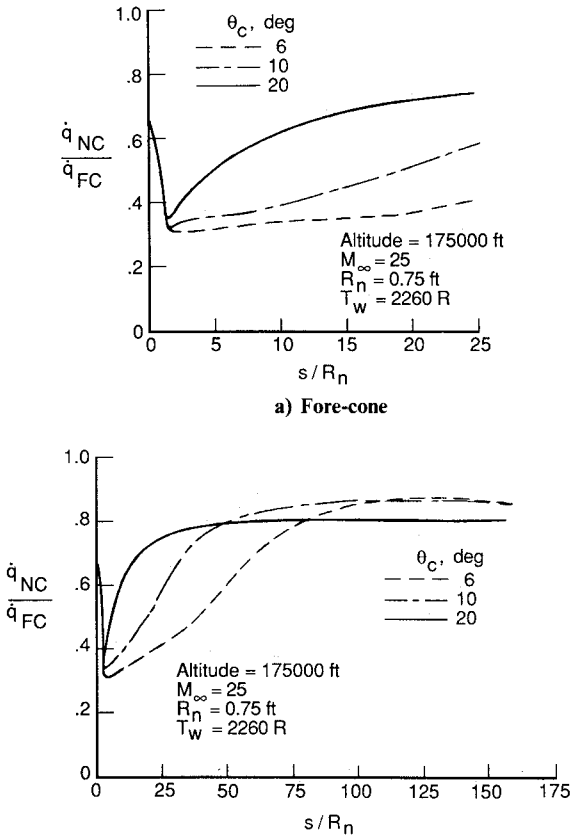

Fig. 3 Cone-angle effect on nonequilibrium heat-transfer distributions, $R_n = 0.75$ ft.

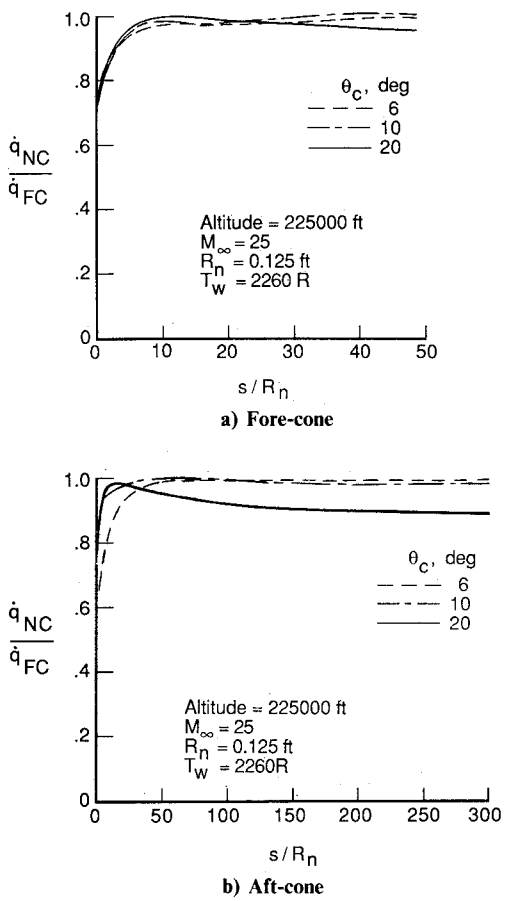

Fig. 4 Cone-angle effect on nonequilibrium heat-transfer distributions, altitude = 225,000 ft.

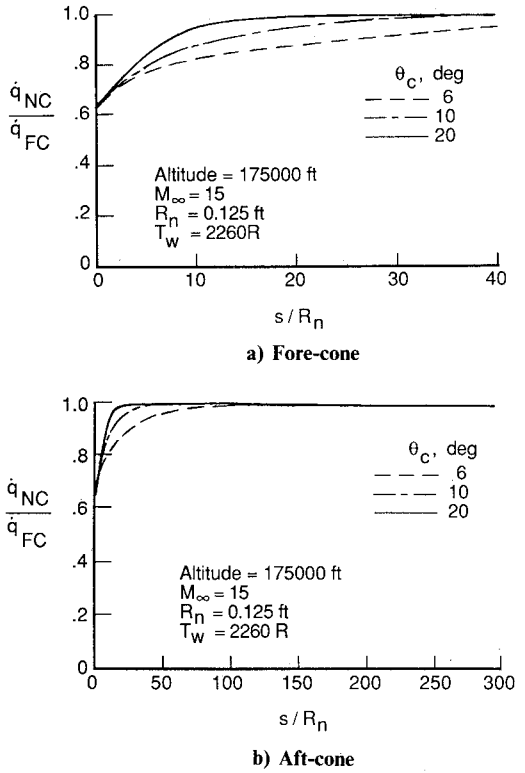

Fig. 5 Cone-angle effect on nonequilibrium heat-transfer distributions, $M_\infty = 15$.

shown[32] to be in good agreement with the Shuttle heating data and the computed results of Ref. 9.

In the initial phases of the current study, preliminary calculations based on the present code and the code described in Ref. 27 were compared. The calculations were for a blunt 6-deg cone at an altitude of 175,000 ft and a Mach number of 25. The results of the comparison indicated that, for the same converged shock shape, the heating rates (comparison of individual noncatalytic and fully catalytic values) were within 10%.

Present Results

The nonequilibrium results of the present parametric study are presented primarily in Figs. 1–5. The nonequilibrium heat-transfer calculations are presented as a ratio of the noncatalytic to fully catalytic heating rates. This ratio is chosen, as previously discussed, to illustrate the maximum potential for a surface heating-rate reduction in the presence of dissociated nonequilibrium flow. However, although the effects of nonequilibrium flow over a surface at a particular freestream condition can be characterized by this ratio, the trends should not be used to infer the actual magnitude of the reduction in heating rates. The effect of the cone half angle on the computed heating ratio is shown at an altitude of 175,000 ft and a freestream Mach number of 25 in Figs. 1–3 for nose radii of 0.125, 0.5, and 0.75 ft, respectively. The influence of cone angle is also shown in Figs. 4 and 5 for a nose radius of 0.125 ft at an altitude of 225,000 ft and a Mach number of 25 and at an altitude of 175,000 ft and a Mach number of 15, respectively. Cone half angles of 6, 10, and 20 deg are used for all of the calculations, and the wall temperature is held constant at 2260°R for most of the conditions.

Cone-Angle Effects

Some general trends with cone angle are observed in the computed results presented in Figs. 1–3. The heating ratios presented for the aft-cone results in Figs. 1b–3b at body stations beyond 100 nose radii indicate a greater potential (as

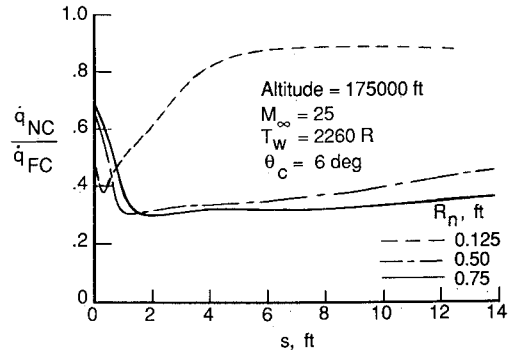

Fig. 6 Nose-radius effect on nonequilibrium heat-transfer distributions, $\theta_c = 6$ deg.

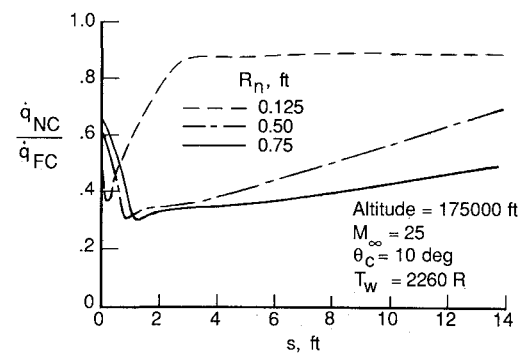

Fig. 7 Nose-radius effect on nonequilibrium heat-transfer distributions, $\theta_c = 10$ deg.

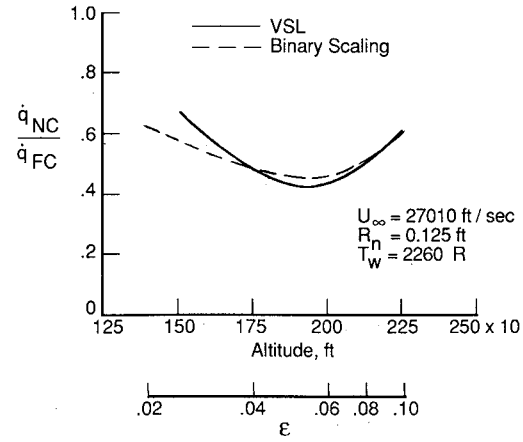

Fig. 8 Altitude effect on stagnation-point nonequilibrium heating.

suggested by a lower value of the ratio) for a heating reduction to the 20-deg cone than the corresponding 6- and 10-deg cones. These results can be attributed to a higher concentration of dissociated species present throughout the flowfield for energy transport by diffusion to the surface for the wider angle cone. In this body region for the lower cone angles, conditions sufficient to produce high concentrations of dissociated species exist only in a small region of the boundary layer. Although these results should have been qualitatively expected, some interesting and possible unexpected trends are observed in the fore-cone results (Figs. 1a–3a) downstream of the cone tangency point. In this region, the largest cone angle produces the smallest nonequilibrium effect as indicated by higher values of the ratio. (This result does not imply that the local or total heating rate to the larger cone angle is less.) This trend may be explained for a given nose radius by considering a selected body station in this region. At the body station, the flow over the smaller cone angles compared to the larger body angle expands rapidly and results in freezing the flow chemistry and corresponding larger percentages of dissociated species.

Mach Number Altitude Effects

Nonequilibrium effects that are computed at different conditions from those of Figs. 1–3 (Mach number of 25 and an altitude of 175,000 ft) are presented in Figs. 4–5. The results in Fig. 4 are calculated for a Mach number of 25 at an altitude of 225,000 ft, whereas the calculations presented in Fig. 5 are for a Mach number of 15 at an altitude of 175,000 ft. The nonequilibrium effects exhibited at the higher altitude (Fig. 4) or the lower Mach number (Fig. 5) conditions are not as large as the results presented in Figs. 1–3. Significant heating reductions are computed primarily in the stagnation regions (Figs. 4a and 5a). The heating-rate ratios increase rapidly from the stagnation point and are greater than 0.9 over most of the cone frustum for any cone angle. For these conditions, a finite-catalytic boundary condition would have little or no influence on the heating. A clarification is also given for the trend of these results. The increasing trend of the ratio does not imply that the individual heating rates increase away from the stagnation region but simply means that the effects of the dissociated species, which are produced primarily in the stagnation region, on the surface heating diminish as the flow spreads over the surface at these conditions.

Bluntness Effects

The computed nonequilibrium heating results have been presented for a variation in cone angle at selected freestream and bluntness conditions. The calculated results are shown in another format in Figs. 6 and 7 to illustrate the nonequilibrium effects for a range of nose radii to a 6- and 10-deg cone, respectively. The heating ratio is shown as a function of the wetted surface distance in the two figures for nose radii of 0.125, 0.5, and 0.75 ft. The possibility of achieving a significant heating reduction in the presence of nonequilibrium dissociated flow is demonstrated for these conditions of increasing bluntness. The potential for a maximum heating reduction of more than 50% is shown in Fig. 6 for the two larger nose radii at running lengths of 14 ft. For the calculations with the 6-deg cone and a 0.75-ft nose radius, a reduction of approximately 50% is feasible at distances of at least 30 ft. The calculated results presented in Fig. 7 for the 10-deg cone also indicate the possibility of a considerable heating reduction.

A comparison of the results in Figs. 6 and 7 implies that the effect of blunting on the heating ratio would not be as significant for larger cone angles. The influence of blunting on the heating ratio for a given cone angle is at least partially explained by the pressure distributions presented in Fig. 9 of Ref. 32. The normalized pressure distributions as a function of surface wetted lengths for a 6-deg cone were shown for nose radii of 0.125 and 0.75 ft. The overexpansion/recompression region occurs rapidly for the smaller nose radius, whereas the region encompasses a much larger portion of the vehicle surface for the 0.75-ft radius. Similar effects were presented in Ref. 3 for perfect-gas solutions and highlight benefits due to blunting. The calculated results of Ref. 3 showed reductions in surface heat transfer (local and total) and drag for a range of nose blunting.

Scaling Effects

Another interesting aspect of the present results is the effect of nose radius or altitude variation on the stagnation-point heat-transfer ratio. The nose radius effect is illustrated directly in either Fig. 6 or Fig. 7, and the altitude effect can be seen by comparing computed stagnation heating ratios in Figs. 1a and 4a. The stagnation-point heating rate is known, for a perfect-gas or equilibrium calculation, to vary approximately as the

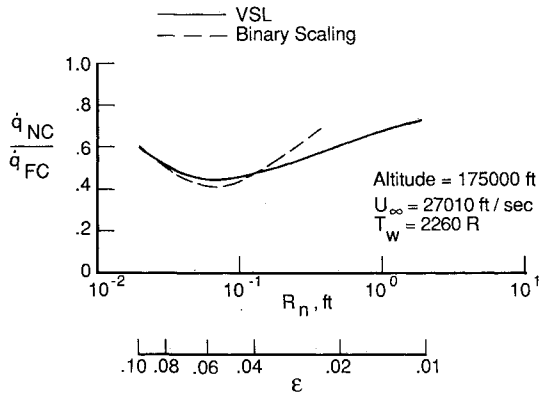

Fig. 9 Nose-blunting effect on stagnation-point nonequilibrium heating.

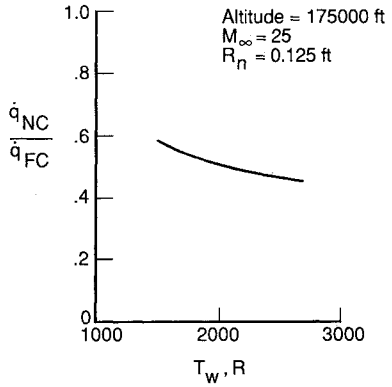

Fig. 10 Wall temperature effect on stagnation-point nonequilibrium heating.

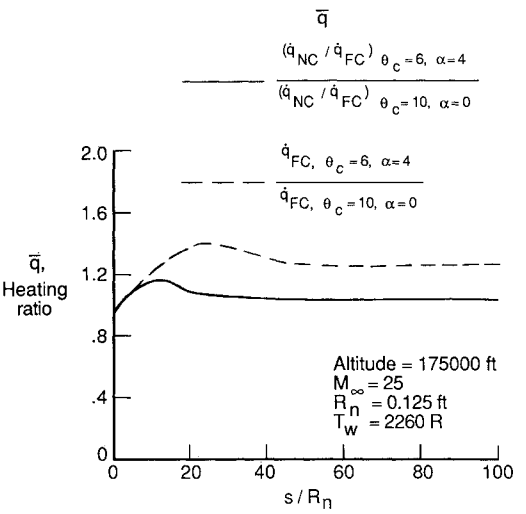

Fig. 11 Angle-of-attack effect on nonequilibrium heat-transfer distributions.

inverse square root of the nose radius and directly as the square root of the freestream density. If the radius can be used independently as a scaling parameter for nonequilibrium flow, then the ratios of heating presented in Figs. 6 and 7 should be independent of the nose radius and, consequently, have the same value. The same reasoning can be made for a density change on the stagnation values presented in Figs. 1a and 4a. Obviously, these parameters cannot be employed independently as scaling parameters because of the differences noted in computed ratios. A possible reason for this lack of scaling is that the thickness of the flowfield disturbance produced by either the bluntness or freestream variations is not the same as the relaxation distance for the chemical reactions in each of the cases. A similitude that has been used for scaling in low-density nonequilibrium flow that is governed by two-body collisions is referred to as binary scaling. Discussions of the applicability of this scaling parameter for air have been presented in Refs. 33–35. A recent study[36] using a Direct Simulation Monte Carlo (DSMC) method provides further application of the binary scaling concept to slender vehicles at low-density conditions. Based on this concept, scaling to a different size body at the same velocity and wall temperature is accomplished by keeping the product of freestream density and nose radius constant.

The interesting nature of the current results is demonstrated by trends shown in Figs. 8 and 9. Additional stagnation-point calculations with the present VSL code have been included with the computed values in Figs. 1–7 to yield the distributions shown in the figures. In Fig. 8, the heating ratio is shown to decrease to a minimum (maximum nonequilibrium effects) and then increase. This trend with increasing altitude is due to the flowfield chemistry changing from an equilibrium state and approaching a frozen state. A similar behavior with increasing nose radius is presented in Fig. 9. However, for a larger nose radius, the flow is approaching an equilibrium state, since the flow distance is becoming large relative to the relaxation distance required for the chemical reactions. The dashed line on each figure represents an effort to assess the binary scaling concept at the present conditions. The VSL-computed heating ratios are presented in Fig. 8 for a constant nose radius as a function of altitude (density), and the corresponding density-radius products can be determined. The computed heating ratios in Fig. 9 are presented at a constant altitude (density) for a range of nose radii. Each heating ratio of Fig. 8 is plotted on Fig. 9 at the radius that satisfies the associated scaling value. A similar approach was used to plot the VSL-computed heating ratios of Fig. 9 on Fig. 8 with binary scaling. Based on the comparisons shown in both figures, the scaling concept is clearly not applicable for the present conditions at ε values less than approximately 0.08 when the three-body recombination reactions begin to influence the flow chemistry. For freestream conditions also characteristic of ε values greater than 0.08, the binary scaling concept was shown in Ref. 36 to produce good correlation of DSMC computations.

Wall Temperature Effects

The influence of wall temperature on the nonequilibrium stagnation-point heating ratio is illustrated in Fig. 10. The computed results imply that for an increasing wall temperature, a larger nonequilibrium stagnation-point heat reduction is obtained. The higher wall temperatures result in higher gas temperatures near the surface and, consequently, slightly more dissociated species. For such a condition, a larger percentage of the heat flux would be due to the diffusion component. Since the assumption of a noncatalytic boundary condition prohibits the contribution due to diffusion, a larger heat reduction is obtained. However, a surface recombination rate for a finite-catalytic surface is also a function of temperature and increases with wall temperature. Thus, higher surface temperatures are not necessarily the most beneficial condition to obtain the largest actual heat reduction. If a surface can be maintained at a temperature by an active cooling process, then a study of the optimum wall temperature would be necessary.

Angle-of-Attack Effects

The impact of angle of attack on the windward-symmetry plane laminar heating distribution has been shown in many investigations[37-39] to be significant, and that the effect is not modeled by employing an equivalent cone method, i.e., using cone angle plus angle of attack. This effect is illustrated also in Fig. 11 by the dashed line. (The calculated results presented in Fig. 11 are based on the method of Ref. 27.) The computed

fully catalytic heating rates for the present condition over a 6-deg cone at a 4-deg angle of attack are a maximum of 40% greater than the corresponding values for a 10-deg cone at a 0-deg angle of attack. A 25% factor is computed over most of the cone frustum. From the perspective of the present investigation, interest may focus on the influence of nonequilibrium flow over the cone at angle of attack relative to the equivalent cone. The solid line in Fig. 11 represents the computed heating-reduction ratio for the cone at angle of attack to the corresponding ratio for the equivalent cone. Generally, the results indicate that the potential heating reduction in nonequilibrium flow is essentially the same over the surface of the two cones. Since the ratio for these conditions is greater than 1, the implication of this result is that the effects of nonequilibrium flow over a cone at angle of attack are less than corresponding effects for the equivalent cone case. The conclusion is based on the fact that the heating-reduction ratio is larger for the angle-of-attack condition. However, the result that the heat-reduction ratio is essentially the same for the two cones should not be construed to mean that angle-of-attack calculations are not necessary for design. The windward-ray heating has been shown to be significantly larger than the equivalent cone values.

Concluding Remarks

The low-altitude ascent phase of a transatmospheric vehicle should provide conditions that determine the thermal protection system of the vehicle. The higher-altitude phase and the entry condition are probably characterized by nonequilibrium heating conditions. A possible design question for these latter conditions is whether surface reradiation is sufficient, or if an active cooling method is needed to maintain desired material temperatures. In past years extensive nonequilibrium studies for the Shuttle were conducted and are contrasted to the limited studies relating to slender vehicles.

A parametric study of nonequilibrium laminar heating effects to slender vehicles has been conducted. The study included the variation of altitude-velocity conditions, blunted cone half angles, and nose bluntness. Cone half angles of 6, 10, and 20 deg with corresponding nose radii of 0.125, 0.5, and 0.75 ft were used. The effects of vehicle attitude and surface temperature were also considered. The heating-rate results were presented as a ratio of the noncatalytic to the corresponding fully catalytic value to illustrate the maximum potential for a heating reduction in dissociated nonequilibrium flow. The heating rate to a finite-catalytic surface would be greater than the noncatalytic value, and thus the actual heating reduction would be less than shown for this study. Also, although the effects of nonequilibrium flow over a surface at a particular freestream condition were characterized by this heating ratio, the relative trends should not be used to infer the actual magnitude of the reduction in heating rates.

When the heating ratios were computed at an altitude of 175,000 ft and a freestream Mach number of 25, and presented as a function of the nondimensional surface distance for each cone angle, the largest effect of nonequilibrium flow was computed for the 20-deg cone. However, the ratio was generally not lower than 0.8. For this cone angle, the finite-rate chemistry produced dissociated species throughout the flowfield, whereas reacting chemistry was only significant in a small region of the boundary layer for the smaller cone angles. In the fore-cone region of these vehicles, the calculations produced an unexpected reversal of this trend. The calculations for the 6-deg cone demonstrated the greatest nonequilibrium effect, and the results were attributed to a more rapid expansion of the flow resulting in freezing of the flow chemistry and larger percentages of dissociated species. An increasing nose radius resulted in larger nonequilibrium effects, i.e., a lower value of the ratio, at a downstream surface distance for a given cone angle. The nonequilibium calculations over the 6-deg cone with a 0.75 ft nose radius resulted in heating reductions of approximately 50% at distances of 30 ft, whereas a corresponding 10% value was computed for a 0.125 ft nose radius.

For the conditions that were considered in the study, the impact of decreasing the freestream Mach number or the freestream density was that significant heating reductions were computed only in the stagnation region. At these conditions, the effects of reacting-gas chemistry were limited primarily to the stagnation region and diminished as the flow spread over the increasing surface areas. The stagnation-point ratios for all of these conditions could not be scaled by the typical dependency on nose radius or freestream density. For nonequilibrium conditions governed by two-body collisions, scaling to another nose radius at the same velocity and wall temperature condition can be accomplished by holding the product of freestream density and nose radius constant. For this study, the effects of nose radius and altitude (density) on the stagnation-point nonequilibrium heating were shown over a range of conditions, and the applicability of binary scaling was demonstrated only over a limited part of this range.

A decreasing value of the wall temperature implied that the most beneficial nonequilibrium results occurred at higher wall temperatures. This result must be incorporated in a design process with the fact that the surface recombination rates for a material also increase with temperature. The effect of angle of attack on the heat-reduction ratio was shown for a condition to be similar to the ratio computed for an equivalent cone angle. However, even if this result is typical of an angle-of-attack condition, calculated results at angle of attack are required for design, since the individual windward-ray heating rates are significantly greater than the corresponding equivalent cone values.

References

[1]Williams, R. M., "National Aerospace Plane: Technology for America's Future," *Aerospace America,* Vol. 24, Nov. 1986, pp. 18–22.

[2]Martin, J. A., et al., "Special Section—Orbit-On-Demand Vehicle," *Aerospace America,* Vol. 23, Feb. 1985, pp. 46–48.

[3]Thompson, R. A., Zoby, E. V., Wurster, K. E., and Gnoffo, P. A., "An Aerothermodynamic Study of Slender Conical Vehicles," AIAA Paper 87-1475, June 1987.

[4]Gupta, R. N., Lee, K. P., Moss, J. N., Zoby, E. V., and Tiwari, S. N., "Viscous Shock-Layer Analysis of Long Slender Bodies," AIAA Paper 87-2487, Aug. 1987.

[5]Lee, K. P., Gupta, R. N., Moss, J. N., Zoby, E. V., and Tiwari, S. N., "Viscous Shock Layer Solutions for the Low-Density Hypersonic Flow Past Long Slender Bodies," AIAA Paper 88-0460, Jan. 1988.

[6]Shinn, J. L., Moss, J. N., and Simmonds, A. L., "Viscous-Shock-Layer Heating Analysis for the Shuttle Windward Plane with Surface Finite Catalytic Recombination Rates," *Progress in Astronautics and Aeronautics: Entry Vehicle Heating and Thermal Protection Systems; Space Shuttle, Solar Starprobe, Jupiter Galileo Probe,* Vol. 85, edited by P. E. Bauer and H. E. Collicott, AIAA, New York, 1983, pp. 149–180.

[7]Rakich, J. V., Stewart, D. A., and Lanfranco, M. J., "Results of a Flight Experiment on the Catalytic Efficiency of the Space Shuttle Heat Shield," *Progress in Astronautics and Aeronautics: Entry Vehicle Heating and Thermal Protection Systems; Space Shuttle, Solar Starprobe, Jupiter Galileo Probe,* Vol. 85, edited by P. E. Bauer and H. E. Collicott, AIAA, New York, 1983, pp. 97–123.

[8]Scott, C. D. and Derry, S. H., "Catalytic Recombination and the Space Shuttle Heating," *Progress in Astronautics and Aeronautics: Entry Vehicle Heating and Thermal Protection Systems; Space Shuttle, Solar Starprobe, Jupiter Galileo Probe,* Vol. 85, edited by P. E. Bauer and H. E. Collicott, AIAA, New York, 1983, pp. 123–149.

[9]Thompson, R. A., "Comparisons of Nonequilibrium Viscous-Shock-Layer Solutions with Windward Surface Shuttle Heating Data," AIAA Paper 87-1473, June 1987.

[10]Kim, M. D., Swaminathan, S., and Lewis, C. H., "Three-Dimensional Viscous Flow Over the Shuttle with Surface Catalytic Effects," AIAA Paper 83-1426, June 1983.

[11]Zoby, E. V., "Technology Development for Slender Body Hypersonic Flowfields," Fourth National Aero-Space Plane Technology Symposium, Monterey, CA, Feb. 1988, Paper 85.

[12]Lee, K. P., "Viscous Shock Layer Analysis of Hypersonic Flows Over Slender Vehicles," Ph.D. Thesis, Old Dominion Univ., Norfolk, VA, Aug. 1988.

[13]Davis, R. T., "Numerical Solution of the Hypersonic Viscous Shock-Layer Equations," *AIAA Journal*, Vol. 8, Dec. 1970, pp. 2152–2156.

[14]Moss, J. N., "Reacting Viscous-Shock-Layer Solutions with Multicomponent Diffusion and Mass Injection," NASA TR-R-411, June 1974.

[15]Blottner, F. G., "Viscous Shock Layer at the Stagnation Point with Nonequilibrium Air Chemistry," *AIAA Journal*, Vol. 7, Dec. 1969, pp. 2281–2288.

[16]Gupta, R. N., "Navier-Stokes and Viscous Shock-Layer Solutions for Radiating Hypersonic Flows," AIAA Paper 87-1576, June 1987.

[17]McBride, B. J., Heimel, S., Ehlers, J. G., and Gordon, S., "Thermodynamic Properties to 6000°K for 210 Substances Involving the First 18 Elements," NASA SP-3001, March 1963.

[18]Esch, D. D., Siripong, A., and Pike, R. W., "Thermodynamic Properties in Polynomial Form for Carbon, Hydrogen, Nitrogen, and Oxygen Systems from 300 to 15,000°K," Louisiana State Univ., Dept. of Chemical Engineering, Reacting Fluids Labs., NASA-FFL-TR-70-3, Nov. 1970.

[19]Browne, W. G., "Thermodynamic Properties of Some Atoms and Atomic Ions," General Electric Co., Missile and Space Vehicle Dept., Engineering Physics, Valley Forge, PA, TM 2, 1962.

[20]Browne, W. G., "Thermodynamic Properties of Some Diatoms and Diatomic Ions," General Electric Co., Missile and Space Vehicle Dept., Engineering Physics, Valley Forge, PA, TM 8, May 1962.

[21]Yos, J. M., private communication, June 1985.

[22]Wilke, C. R., "A Viscosity Equation for Gas Mixtures," *Journal of Chemical Physics,* Vol. 18, April 1950, pp. 517–519.

[23]Mason, E. A. and Saxena, S. C., "Approximate Formula for the Thermal Conductivity of Gas Mixtures," *Physics of Fluids,* Vol. 1, No. 5, Sept.–Oct. 1958, p. 361.

[24]Waskiewicz, J. D., Murray, A. L., and Lewis, C. H., "Hypersonic Viscous Shock-Layer Flow Over a Highly Cooled Sphere," *AIAA Journal,* Vol. 16, Feb. 1978, pp. 189–192.

[25]Murray, A. L. and Lewis, C. H., "Hypersonic Three-Dimensional Viscous Shock Layer Flows Over Blunt Bodies," *AIAA Journal,* Vol. 16, Dec. 1978, pp. 1279–1286.

[26]Szema, K. Y., Thareja, R. R., and Lewis, C. H., "Three-Dimensional Viscous Shock-Layer Flows Over Lifting Bodies at High Angle of Attack," AIAA Paper 81-1146, June 1981.

[27]Swaminathan, S., Kim, M. D., and Lewis, C. H., "Three-Dimensional Nonequilibrium Viscous Shock-Layer Flows Over Complex Geometries," AIAA Paper 83-0212, Jan. 1983.

[28]Adams, J. C., Martindale, W. R., Mayne, A. W., Jr., and Marchand, W. O., "Real Gas Scale Effects on Hypersonic Laminar Boundary-Layer Swallowing," Arnold Engineering Development Center, Arnold AFS, TN, AEDC-TR-75-2, Dec. 1975.

[29]Zoby, E. V., "Approximate Heating Analysis for the Windward-Symmetry Plane for Shuttle-Like Bodies at Large Angle of Attack," *Progress in Astronautics and Aeronautics: Thermophysics of Atmospheric Entry*, Vol. 82, edited by T. E. Horton, AIAA, New York, 1982, pp. 229–247.

[30]Zoby, E. V., "Analysis of STS-2 Experimental Heating Rates and Transition Data," *Journal of Spacecraft and Rockets,* Vol. 20, May–June 1983, pp. 232–237.

[31]Thompson, R. A., "Three-Dimensional Viscous-Shock-Layer Application for the Space Shuttle Orbiter," *Progress in Astronautics and Aeronautics: Thermophysical Aspects of Re-entry Flows*, Vol. 103, edited by J. N. Moss and C. D. Scott, AIAA, New York, 1986, pp. 541–570.

[32]Zoby, E. V., Lee, K. P., Gupta, R. N., Thompson, R. A., and Simmonds, A. L., "Viscous Shock-Layer Solutions with Nonequilibrium Chemistry for Hypersonic Flows Past Slender Bodies," AIAA Paper 88-2709, June 1988.

[33]Ellington, D., "Binary Scaling Limits for Hypersonic Flight," *AIAA Journal*, Vol. 5, Sept. 1967, pp. 1705–1706.

[34]Vidal, R. J., "High Temperature Phenomena in Hypersonic Flows—Final Report," AEDC-TRD-64-143, June 1984.

[35]Birkhoff, G., "Fact, Logic, and Similitude," Princeton Univ. Press, Princeton, NJ, 1960, p. 109.

[36]Moss, J. N., Cuda, V., and Simmonds, A. L., "Nonequilibrium Effects for Hypersonic Transitional Flows," AIAA Paper 87-0404, Jan. 1987.

[37]Widhopf, G. F., "Turbulent Heat-Transfer Measurements on a Blunt Cone at Angle of Attack," *AIAA Journal*, Vol. 9, Aug. 1971, pp. 1574–1580.

[38]Heins, A. E. and Estes, T. J., "Effects of Angle of Attack on Laminar Convective Heat Transfer on Sharp and Blunt Cones," General Electric, Philadelphia, PA, TIS 61SD70, April 1961.

[39]Adams, J. C., Jr., "Implicit Finite-Difference Analysis of Compressible Laminar, Transitional, and Turbulent Boundary Layers Along the Windward Streamline on a Sharp Cone at Incidence," Arnold Engineering Development Center, Arnold AFS, TN, AEDC-TR-71-235, Dec. 1971.